



hal-00141682, version 1 - 13 Apr 2007

Arnaud Ralko,¹ Frédéric Mila,² and Didier Poilblanc¹

¹ *Laboratoire de Physique Théorique, CNRS & Université Paul Sabatier, F-31062 Toulouse, France*

² *Institute of Theoretical Physics, Ecole Polytechnique Fédérale de Lausanne (EPFL), CH-1015 Lausanne, Switzerland*

(Dated: April 5, 2007)

The doped two-dimensional quantum dimer model is investigated by numerical techniques on the square and triangular lattices, with significantly different results. On the square lattice, at small enough doping, there is always a phase separation between an insulating valence-bond solid and a uniform superfluid phase, whereas on the triangular lattice, doping leads directly to a uniform superfluid in a large portion of the RVB phase. Under an applied Aharonov-Bohm flux, the superfluid exhibits quantization in terms of half-flux quanta, consistent with $Q = 2e$ elementary charge quanta in transport properties.

PACS numbers: 75.10.Jm, 05.50.+q, 05.30.-d

Understanding electron pairing in high temperature superconductors is a major challenge in strongly correlated systems. In his milestone paper, Anderson proposed a simple connection between high temperature superconductors and Mott insulators [1]. Electron pairs "hidden" in the strongly correlated insulating parent state as Valence Bond (VB) singlets lead, once freed to move at finite doping, to a superconducting behavior. A very good candidate of the insulating parent state is the resonating VB state (RVB), a state with only exponentially decaying correlations and no lattice symmetry breaking. A simple realization of RVB has been proposed by Rokhsar and Kivelson (RK) in the framework of an effective quantum dimer model (QDM) with only local processes and orthogonal dimer coverings [2]. Even though the relevance of these models for the description of SU(2) Heisenberg models is not fully established, this approach is expected to capture the physics of systems that naturally possess singlet ground states (GS). Indeed, specific quantum dimer models have recently been derived from a spin-orbital model describing LiNiO₂ [3], or from the trimerized *kagome* antiferromagnet [4]. In a recent work, a family of doped QDMs (at T=0) generalizing the so-called RK point of Ref.[2] has been constructed [5], taking advantage of a mapping to classical dimer models [6] that extends the mapping of the RK model onto a classical model at infinite temperature. This investigation has suggested that phase separation into two macroscopic constituents, an undoped phase and a phase with larger doping, could be quite generic in doped QDMs [5]. Despite their *ad-hoc* construction, the "quasi-classical" QDMs of Ref.[5] are expected to reflect many features of more realistic models such as the two-dimensional quantum hard-core dimer-gas defined by the Hamiltonian:

$$H = v \sum_c N_c |c\rangle \langle c| - J \sum_{(c,c')} |c'\rangle \langle c| - t \sum_{(c,c'')} |c''\rangle \langle c| \quad (1)$$

where the sum on (c) runs over all configurations of the

Hilbert space, N_c is the number of flippable plaquettes, the sum on (c', c) runs over all configurations $|c\rangle$ and $|c'\rangle$ that differ by a single plaquette dimer flip, and the sum on (c'', c) runs over all configurations $|c\rangle$ and $|c''\rangle$ that differ by a single hole hopping (see Ref. [5] for more details). Throughout the energy scale is set by $J = 1$. A schematic phase diagram for the two lattices is depicted in Fig.1 in the undoped case. Remarkably, these lattices lead to quite different insulating states. Indeed, an ordered plaquette phase appears on the square lattice immediately away from the special RK point, whereas a RVB liquid phase is present in the triangular lattice

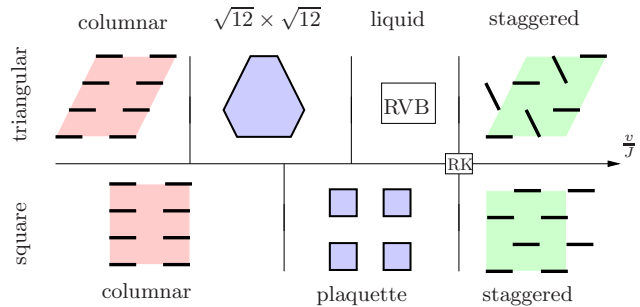


FIG. 1: (color online) Schematic phase diagrams for the triangular and the square lattice.

In this Letter, we investigate in details the properties of model (1) on the square and triangular lattices at finite doping. Building on the differences between the two lattices in the undoped case, we investigate to which extent the properties of the doped system are governed by the nature of the insulating parent state. This investigation is based on exact Diagonalisations and extensive Green's Function Monte-Carlo (GFMC) simulations [7, 8], particularly well adapted for QDM for which all off-diagonal elements are non-positive. [9].

Phase separation: At small t , it is expected that holes experience an effective attractive potential. It is there-

fore natural to first address the issue of phase separation (PS), *i.e.* the possibility for the system to spontaneously undergo a macroscopic segregation into two phases with different hole concentrations. We analyze the problem as a function of the hopping parameter t and hole concentration $x = n_h/N$, where n_h is the number of holes in the system and N the number of sites. In order to perform a Maxwell construction (see for example [10]) we define:

$$s(x) = \frac{e(x) - e(0)}{x} \quad (2)$$

where $e(x)$ is the energy per site at doping x . This quantity corresponds to the slope of the line passing through $e(0)$ and $e(x)$. If the system exhibits PS, the energy will present a change of curvature implying $s(x)$ to have a minimum at a critical doping x_c . The fact that the local curvature of $e(x)$ at $x = 0$ is negative then implies that the two separated phases will have $x = x_c$ and $x = 0$ (the undoped insulator). In Fig.2, typical results are shown for both square and triangular lattices and for different sizes. Interestingly, PS appears in both cases, but with

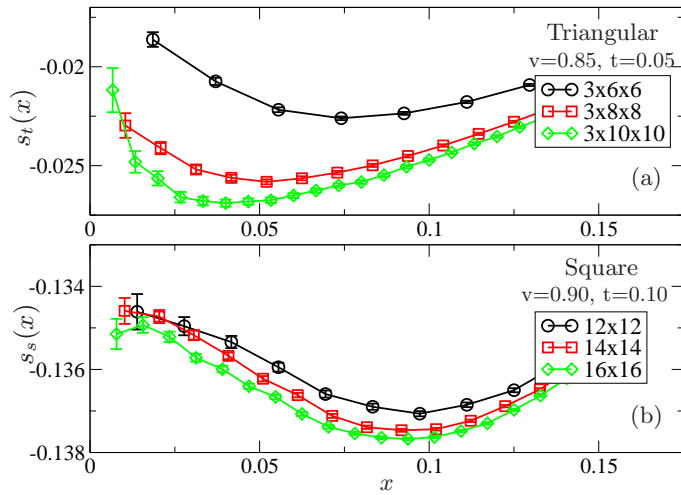


FIG. 2: (color online) Slope of energy density (Eq.(2)) vs doping for different sizes. (a) Triangular lattice. (b) Square lattice.

noticeable differences. While for the square lattice (lower panel) the critical hole concentration x_c is roughly size independent, there is a strong size dependence for the triangular lattice (upper panel). This size effect can be traced back to the nature of the parent undoped state. On the square lattice, the crystalline phase (for $v < 1$) at zero doping is very robust and for increasing size, its local order changes only weakly. On the triangular lattice, it has been shown that size effects play an important role [9], especially in the RVB liquid phase for $0.8 \lesssim v \leq 1$. Periodic boundary conditions tend to stabilize the so-called $\sqrt{12} \times \sqrt{12}$ phase on small clusters, and clusters with more than 192 sites are necessary to significantly reduce finite-size effects, in particular, as in Fig.2, close

to the transition point with the crystalline phase. Hence the PS observed around $x = 0.075$ for the $3 \times 6 \times 6$ cluster is not representative of the thermodynamic limit.

To obtain the phase diagram in the (v, x) plane, we have performed a systematic size-scaling analysis at fixed t and for various v 's depicted in Fig.3. In agreement with

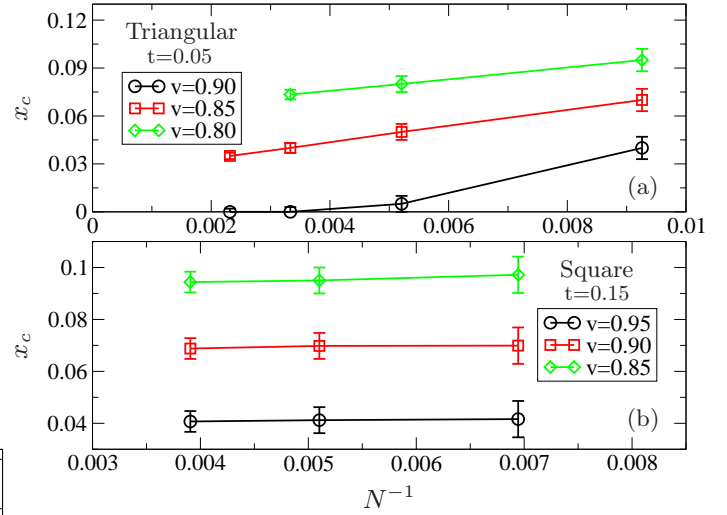


FIG. 3: (color online) Scaling of the critical doping x_c defined by Maxwell construction with the inverse total number of sites. (a) Triangular lattice. (b) Square lattice.

the previous discussion, a significant size dependence is only present for the triangular lattice, in which case PS disappears for large clusters in the RVB phase in the vicinity of the RK point [11]. In Fig.4, we report the thermodynamic limit of x_c for the two lattices as a function of v , and for different values of t . For the square lattice, calculations have been done from the RK point down to the expected phase transition between the plaquette phase and the columnar phase, namely $v \simeq 0.6$ [12]. For the triangular lattice, the range between the RK point down to the RVB- $\sqrt{12} \times \sqrt{12}$ transition point at $v \simeq 0.8$ has been covered [9]. These results clearly demonstrate the difference between the square and triangular lattices. In the first case, as soon as $v \neq 1$, PS occurs for $x < x_c$. Moreover, upon decreasing v , crystalline order strengthens and, for fixed t , it is necessary to consider a higher concentration of holes to reach a stable conducting phase. Similarly, the bigger t , the lower x_c . On the triangular lattice, a finite size-scaling analysis shows that no phase separation appears down to a critical value $v \sim 0.9$, well above the critical value $v \sim 0.8$ below which plaquette order sets in. Although numerical limitations prevent computations for smaller v and t , our results up to the $3 \times 12 \times 12$ -site cluster provide clear evidence for a region of PS inside the RVB region, between $v \sim 0.8$ and $v \sim 0.9$.

Dimer ordering on the square lattice: Next we investi-

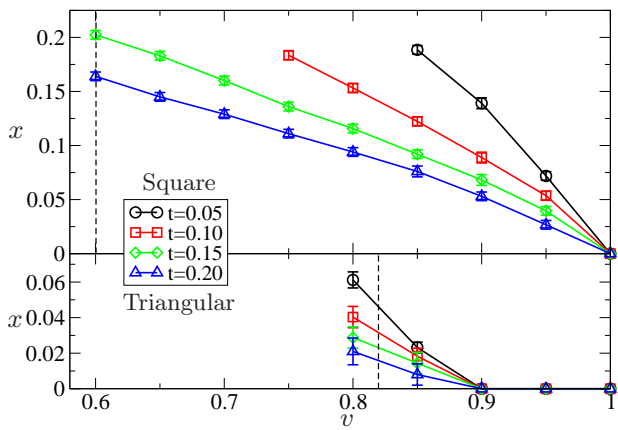


FIG. 4: (color online) Phase separation boundaries for the square and triangular lattices in the thermodynamic limit. The dashed lines correspond to the approximate location of the phase transition between plaquette and columnar phases [12] for the square lattice and between plaquette and RVB phases [9, 13] for the triangular lattice.

gate how dimer order, known to exist at $x = 0$, evolves under finite doping. Two scenarios are *a priori* possible: i) the dimer order vanishes in the stable conducting phase immediately at x_c ; ii) dimer order survives above x_c in a narrow region of the conducting phase. To solve this problem, we have calculated the squared order parameter $D^2(\vec{k})$ defined by:

$$D^2(\vec{k}) = \frac{1}{N} \frac{\langle \Psi_0 | d(-\vec{k}) d(\vec{k}) | \Psi_0 \rangle}{\langle \Psi_0 | \Psi_0 \rangle} \quad (3)$$

along the path $\Gamma \rightarrow M \rightarrow K \rightarrow \Gamma$ in the first Brillouin zone of the square lattice, using standard notations, where $d(\vec{k})$ is the Fourier transform of the dimer operator d_i in the \vec{u}_x direction which multiplies a configuration by 1 if there is dimer between site i and its right neighbor, and 0 otherwise. Note that this calculation has not been tried for the triangular lattice since no Bragg peak is present in the RVB phase, and the algorithm is losing efficiency for $v \lesssim 0.8$ [11]. In the pure plaquette phase on the square lattice, a Bragg peak develops at point $\vec{k}_M = (\pi, 0)$, the middle of the side of the BZ. We show in the inset of Fig.5 a typical result for the squared order parameter on the 196-site cluster for different values of x . Clearly, the Bragg peak disappears upon doping. A finite size scaling of the order parameter can be performed thanks to the linear behaviour at low concentration. Within our data, $D^2(\vec{k} = \vec{k}_M) \equiv D_M^2(L, x)$ behaves like $a_L x + b_L$ in the linear region. In this case, one can determine rather precisely $x_{+\infty}$ such that $D_M^2(+\infty, x_{+\infty}) = 0$ *i.e.* $x_{+\infty}$ is the concentration in the thermodynamic limit where the Bragg peak vanishes. By definition, $x_{+\infty} = -b_{+\infty}/a_{+\infty} \simeq 0.05(8)$. This value, and the linear behaviour in the thermodynamic limit, are

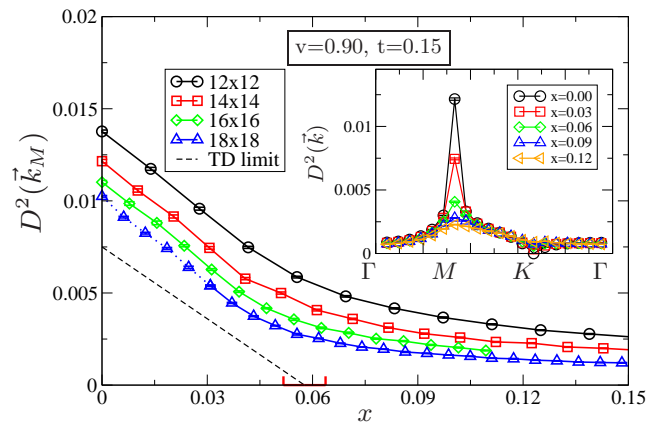


FIG. 5: (color online) Squared order parameter at the M point as a function of the hole concentration x and for different cluster sizes. The thermodynamic limit is depicted as a dashed line, with the corresponding error bar (see main text). Inset: Momentum dependence of the squared order parameter for the 196-site cluster (14x14).

displayed in Fig.5. If we compare $x_{+\infty}$ to the corresponding x_c from Fig.4, we can conclude that the Bragg peak indeed vanishes at $x_c \simeq 0.067(5)$ within error bars. Note that numerical errors increase for larger clusters, and we are not able to use the same analysis for clusters larger than 256 sites (the results for the 18×18 cluster have not been used). Although the determination of $x_{+\infty}$ is delicate, the linear behavior of D^2 vs x is consistent with the physical behavior expected for the binary system of Fig.4. No dimer order is present above x_c , showing that the system is simply “conducting” in this case.

Flux quantization: Finally, let us turn to a better characterization of the “conducting phase”. In the model defined by the Hamiltonian of Eq.(1), the holes are bosonic, and we therefore expect the conducting phase to be a superfluid (through Bose condensation)[14]. However, since these bosons move in a dimer environment, pair correlations might be present. To investigate this issue, we pierce the torus by an Aharonov-Bohm flux of strength $\phi = 2\pi\xi$ with $0 \leq \xi \leq 1$. The flux is simply implemented by the Peierls substitution, changing the hole hopping term into $t' = \exp(\pm i2\pi\xi/L_x)t$, where the \pm depends on whether the hole hops to the right or to the left, and where L_x is the linear size of the system. Obviously, the whole spectrum should be periodic in ξ with period 1. We show in Fig.6 the spectrum of the 4×4 cluster on the square lattice, with 4 holes. It turns out that the spectrum is rigorously periodic with period $\xi = 1/2$, which means that there is flux quantization in units of *half* the flux quantum (red curve). This was suggested quite some time ago in the context of a more general QDM by Kivelson[14], who also predicted that, in the cylinder geometry, one can in principle tunnel between

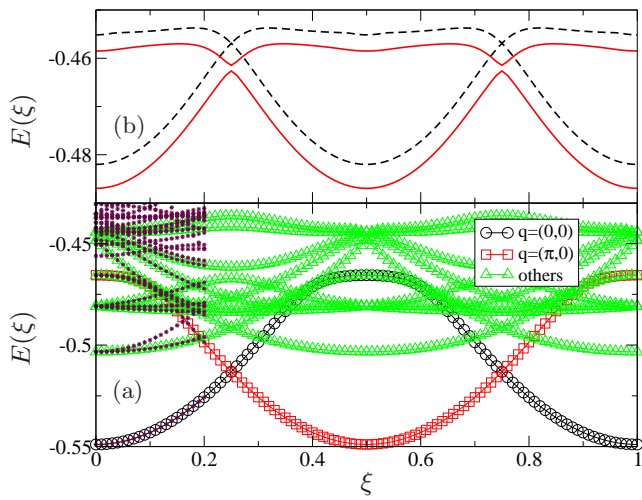


FIG. 6: (color online) Energy spectrum vs (reduced) Aharonov-Bohm flux ξ , for a 4×4 cluster with 4 holes at $v = 0.70$ and $t = 1.00$. (a) Torus geometry. The momenta of the two low-energy branches are specified and the complete spectrum is displayed up to $\xi = 0.2$. (b) The two low-energy branches for the case of a cylinder (dashed line) and including a small bond disorder (full red line).

the two branches of Fig.6 by creating finite energy vortex-antivortex excitations that are finally pulled off through the edges of the cylinder, lifting the degeneracy at the level crossing. This lifting of degeneracy is not present in our case, neither in the torus geometry, nor in the cylinder geometry. However, this is just a consequence of the translational symmetry, which puts the two states that are degenerate at $\xi = 1/4$ into different symmetry sectors. Removing the translational symmetry by changing the amplitude of a local dimer flip indeed removes the degeneracy (upper panel of Fig.6). In that case, the flux quantization in units of half the flux quantum could indeed be detected in an experiment in which the flux is swepted. Thus, in our model, the ground-state energy has periodicity $hc/2e$, suggesting the presence of mobile pairs (or elementary particles of charge $Q = 2e$) in the system[10]. Note that, unlike what was recently found in a bosonic model with correlated hopping[15], these particles are probably not boson pairs (although a definite proof would require the knowledge of the two particle Green's function not accessible with GFMC, boson pairs are unlikely, at least far enough from the phase separation): From the bosonic point of view, it is the statistical flux of the dimer background that leads to the half-flux quantization. If dimers are interpreted as SU(2) electron singlets, these singlets are the physical pairs that lead to half-flux quantization.

Summary and conclusions: The numerical investigation with Green's function Quantum Monte Carlo and exact diagonalizations of the doped two-dimensional quantum hard-core dimer model on the square and triangular

lattices has led to a number of interesting conclusions regarding hole motion in a dimer background. Phase separation is often present at low doping, as suggested by earlier investigations, but our results indicate that it related to the presence of valence bond order: In the RVB phase of the triangular lattice, PS only occurs close to the plaquette phase, where short-range dimer correlations are already strong enough. Close to the RK point, doping the RVB phase leads directly to a conducting (most likely superfluid) phase. To characterize this phase, we have studied the effect of an Aharonov-Bohm flux, with the conclusion that the flux quantization is in units of half a flux quantum, consistent with the idea that the dimer background leads to effective particles of charge $2e$. All these results are in qualitative agreement with the gauge theories of high T_c superconductivity in strongly correlated systems [16]. Finally, let us emphasize that, thanks to the large sizes that we could simulate with GFMC, all these conclusions are essentially free of the usual finite-size limitations of the numerical investigation of strongly correlated electron models.

We acknowledge useful discussions with Federico Becca. This work was supported by the Swiss National Fund, by MaNEP, and by the Agence Nationale de la Recherche (France).

-
- [1] P.W. Anderson, *Science* **235**, 1196 (1987).
 - [2] D.S. Rokhsar and S.A. Kivelson, *Phys. Rev. Lett.* **61**, 2376 (1988).
 - [3] F. Vernay, A. Ralko, F. Becca and F. Mila, *Phys. Rev. B* **74**, 054402 (2006).
 - [4] M. E. Zhitomirsky, *Phys. Rev. B* **71**, 214413 (2005).
 - [5] D. Poilblanc, F. Alet, F. Becca, A. Ralko, F. Trouselet and F. Mila, *Phys. Rev. B* **74**, 014437 (2006).
 - [6] C. Castelnovo, C. Chamon, C. Mudry and P. Pujol, *Ann. Phys.* **322**, 903 (2007).
 - [7] N. Trivedi and D.M. Ceperley, *Phys. Rev. B* **41**, 4552 (1990).
 - [8] M. Calandra and S. Sorella, *Phys. Rev. B* **57**, 11446 (1998).
 - [9] A. Ralko, M. Ferrero, F. Becca, D. Ivanov, and F. Mila, *Phys. Rev. B* **71**, 224109 (2005). *Ibid*, *Phys. Rev. B* **74**, 134301 (2006). F. Vernay, A. Ralko, F. Becca, and F. Mila, *Phys. Rev. B* **74**, 054402 (2006).
 - [10] D. Poilblanc, *Phys. Rev. B* **52**, 9201 (1995).
 - [11] For small values of t , the GFMC algorithm is no longer ergodic due to hole localization, which introduces a bias in the sampling.
 - [12] O.F. Syljuasen, *Phys. Rev. B* **71**, 020401(R) (2005).
 - [13] R. Moessner and S. L. Sondhi, *Phys. Rev. B* **63**, 224401 (2001).
 - [14] S. Kivelson, *Phys. Rev. B* **39**, 259 (1989).
 - [15] R. Bendjama, B. Kumar, F. Mila, *Phys. Rev. Lett.* **95**, 110406 (2005).
 - [16] T. Senthil and P.A. Lee, *Phys. Rev. B* **71**, 174515 (2005) and references therein.